Nanoscale

PAPER

View Article Online
View Journal | View Issue

Cite this: *Nanoscale*, 2014, **6**, 13761

Boron dipyrromethene (BODIPY) functionalized carbon nano-onions for high resolution cellular imaging†

Juergen Bartelmess,[a] Elisa De Luca,[b] Angelo Signorelli,[a] Michele Baldrighi,[a] Michele Becce,[a] Rosaria Brescia,[c] Valentina Nardone,[d,e] Emilio Parisini,[d] Luis Echegoyen,[f] Pier Paolo Pompa[b] and Silvia Giordani*[a]

Received 7th August 2014,
Accepted 10th September 2014

DOI: 10.1039/c4nr04533e

www.rsc.org/nanoscale

Carbon nano-onions (CNOs) are an exciting class of carbon nanomaterials, which have recently demonstrated a facile cell-penetration capability. In the present work, highly fluorescent boron dipyrromethene (BODIPY) dyes were covalently attached to the surface of CNOs. The introduction of this new carbon nanomaterial-based imaging platform, made of CNOs and BODIPY fluorophores, allows for the exploration of synergetic effects between the two building blocks and for the elucidation of its performance in biological applications. The high fluorescence intensity exhibited by the functionalized CNOs translates into an excellent *in vitro* probe for the high resolution imaging of MCF-7 human breast cancer cells. It was also found that the CNOs, internalized by the cells by endocytosis, localized in the lysosomes and did not show any cytotoxic effects. The presented results highlight CNOs as excellent platforms for biological and biomedical studies due to their low toxicity, efficient cellular uptake and low fluorescence quenching of attached probes.

Introduction

In the flourishing research field of nanomedicine, the outstanding results provided by carbon nanomaterials continuously stimulate their improvement in different areas, such as regenerative medicine, drug delivery and bioimaging.[1–3] For these purposes, fullerenes,[4–6] carbon nanotubes,[7,8] nanodiamonds[9,10] and graphene based nanostructures[11,12] have recently been investigated, providing excellent results and showing, in some cases, the possibility of combining multiple features on a single nano-platform.[1] In the search for the best (*i.e.* the most effective and the least toxic) nano-vector, carbon nano-onions (CNOs)[13] have played, until now, only a minor role. Their possible application in nanomedicine has not been fully explored, despite extensive investigations in other fields of research,[14] such as tribology,[15,16] sensing,[17,18] catalysis,[19] and their use in supercapacitors.[20–22] Their application in the context of biomedicine is limited to very few examples,[17,23] in which few-layered (≈5 nm average diameter) CNOs have demonstrated very promising properties in cell penetration, along with low cytotoxicity and low inflammatory potential.[23] Furthermore, following synthetic strategies developed for other carbon nanomaterials,[24] pristine CNOs (**p-CNOs**) can be decorated with a large variety of functional groups.[14,25] A common reaction for covalent CNO functionalization is the so-called *Tour* reaction,[26] which allows for the introduction of a large variety of functional groups,[25] for example benzoic acid.

The fluorescent tag used in this study is a boron dipyrromethene (BODIPY) derivative. BODIPY dyes show excellent optical properties like high molar extinction coefficients as well as high fluorescence quantum yields in combination with good stability.[27,28] They are therefore widely used as imaging agents in biology.[29–31] In addition, the application of BODIPY dyes in systems for solar energy conversion,[32–35] light-driven hydrogen generation,[36] and for photodynamic therapy of cancer[37,38] has been studied. Electrogenerated chemilumines-

[a]*Istituto Italiano di Tecnologia (IIT), Nano Carbon Materials, Nanophysics Department, Via Morego 30, 16163 Genova, Italy. E-mail: silvia.giordani@iit.it; Tel: +39-010-71781-507*
[b]*Istituto Italiano di Tecnologia (IIT), Center for Bio-Molecular Nanotechnology, Via Barsanti, 73010 Arnesano (Lecce), Italy*
[c]*Istituto Italiano di Tecnologia (IIT), Nanochemistry Department, Via Morego 30, 16163 Genova, Italy*
[d]*Istituto Italiano di Tecnologia (IIT), Center for Nano Science and Technology (CNST), Via G. Pascoli 70/3, 20133 Milano, Italy*
[e]*Department of Chemistry, Materials and Chemical Engineering "Giulio Natta", Politecnico di Milano, Via Mancinelli 7, 20131 Milano, Italy*
[f]*Department of Chemistry, University of Texas at El Paso, 500 W. University Ave., El Paso, TX 79968, USA*

†Electronic supplementary information (ESI) available: Additional experimental and crystallographic data, additional confocal microscopy and HR-TEM images and illustrations, EELS, TGA, DLS and Z-potential results. Movie M1. See DOI: 10.1039/c4nr04533e

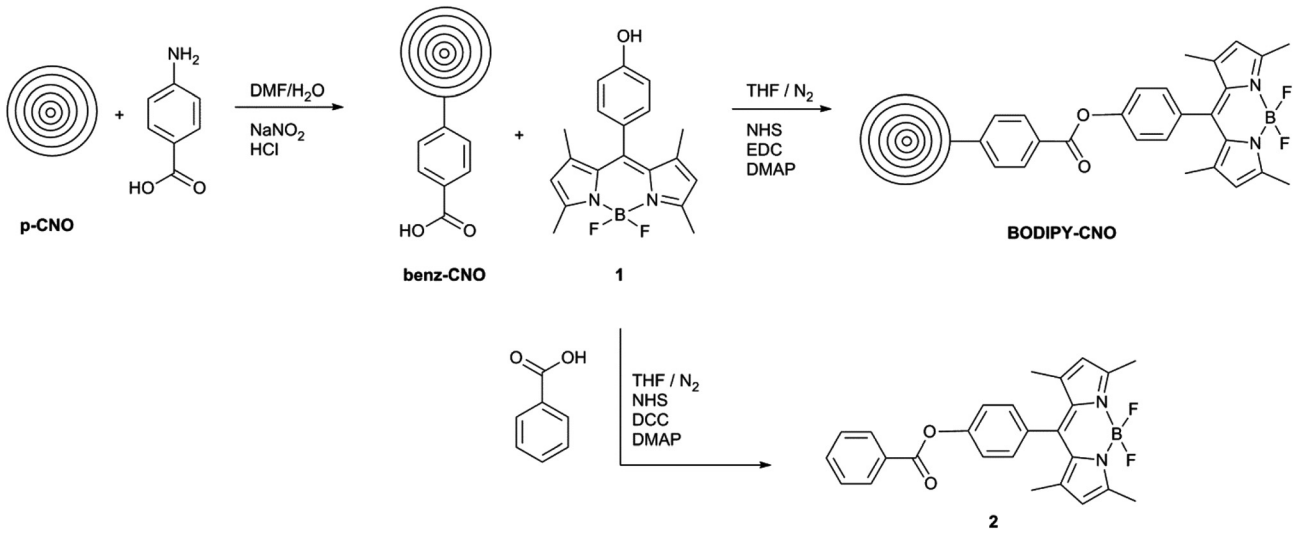

Scheme 1 Synthetic procedure for the synthesis of BODIPY functionalized CNOs (**BODIPY-CNO**) and the corresponding benzoic acid ester (**2**).

cence[39] and fluorescence sensing[40] have also been described for a variety of BODIPY derivatives. The synthetic versatility of the BODIPY chromophore is well documented and allows for a wide range of structural modifications, altering the dyes' electronic, optical and chemical properties.[27,28,41,42]

In earlier studies, the further functionalization of carboxylic or benzoic acid decorated CNOs was accomplished by condensation reactions with primary amines leading to amides.[14,17,23] In the present study, we report for the first time the esterification of benzoic acid functionalized small diameter (≈5 nm) CNOs with the *meso*-phenol substituted boron dipyrromethene (BODIPY) fluorophore **1**.[43] To the best of our knowledge, this is also the first report of the use of a *meso*-phenol substituted BODIPY as a substrate for a Steglich-type esterification reaction with benzoic acid derivatives. All carbon nanomaterials were characterized by means of Raman spectroscopy and attenuated total reflectance Fourier transform infrared spectroscopy (ATR-FTIR), thermogravimetric analysis (TGA), UV-vis absorption and fluorescence spectroscopy, dynamic light scattering (DLS), Z-potential, low and high resolution transmission electron microscopy (LRTEM and HRTEM), electron energy loss spectroscopy (EELS) and atomic force microscopy (AFM). The cellular uptake mechanisms of the CNO nanomaterials by MCF-7 (Michigan Cancer Foundation-7) breast cancer cells and the intracellular localization of the fluorescent CNOs were elucidated. In combination with toxicological studies, this work highlights the excellent properties of CNO based nanomaterials for biological imaging and encourages future studies with CNOs as molecular shuttles for targeted drug delivery.

Results and discussion

Synthetic aspects

BODIPY functionalized CNOs (**BODIPY-CNO**s) and the related benzoic acid-BODIPY ester **2**, used as reference compound, were synthesized by an ester condensation reaction (Scheme 1). The raw CNO material (**p-CNO**) was prepared by the annealing of nanodiamond particles with a diameter of approx. 5 nm, following reported procedures.[44–46] Benzoic acid functionalities were introduced by reacting **p-CNO**s with 4-aminobenzoic acid and sodium nitrite in an acidified DMF/water mixture, an adaptation of the *Tour* reaction.[23,25,26] Subsequently, **benz-CNO**s were reacted with *N*-hydroxysuccinimide (NHS) and the *meso*-phenol substituted BODIPY **1**.[43] The esterification reaction was carried out in the presence of 1-ethyl-3-(3-dimethylaminopropyl) carbodiimide (EDC) (or *N*,*N*′-dicyclohexylcarbodiimide – DCC, as indicated in Scheme 1) and 4-(dimethylamino)pyridine (DMAP) in dry THF. The **BODIPY-CNO** nanomaterial was purified by subsequent centrifugation and several re-dispersion steps in THF, while **2** was purified by column chromatography.

Reference compound 2

The reference compound **2** was synthesized to study the spectroscopic properties of this new BODIPY fluorophore without being influenced by the presence of the CNO nanomaterial. In general, a close connection between carbon nanomaterials and chromophores makes it difficult to investigate the properties of the bound chromophore in great detail. Usually, a broadening and weakening of the fluorescence signal is observed, mainly due to the size and strong intrinsic absorption of the carbon nanostructures and possible electronic interactions.[23,47,48]

X-ray quality crystals of **2** were obtained as orange rhombic plates by re-crystallization from dichloromethane–methanol (1 : 3 v/v) at −20 °C. The diffraction derived structure of **2** is presented in Fig. 1;‡ additional details, tables and a number-

‡Crystallographic data for **2**: CCDC 1015701, $C_{26}H_{23}N_2O_2F_2B$, M = 444.27, orthorhombic F, a = 18.4695(18), b = 43.010(4), c = 10.9507(11) Å, $\alpha = \beta = \gamma = 90°$, V = 8699.0(15) Å^3, T = 100 K, space group $Fdd2$, Z = 16, 6167 reflections measured, 2757 independent (R_{int} = 0.043). The final w$R(F_2)$ was 0.154.

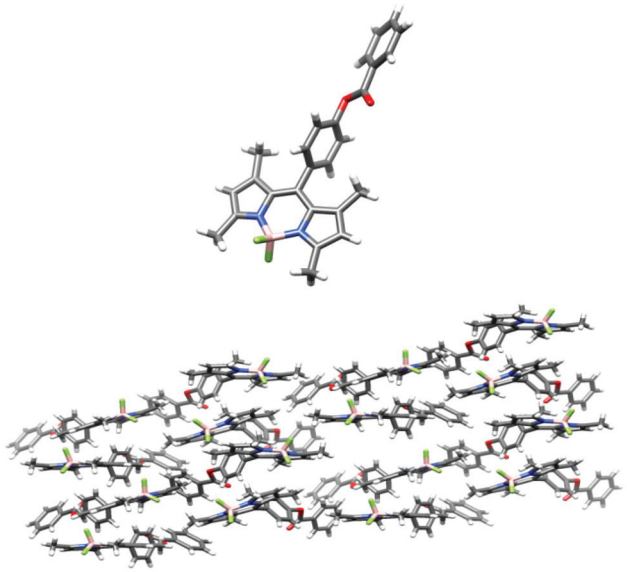

Fig. 1 Crystal structure of **2**. Structure of a single BODIPY-ester molecule (top) and the remarkable high-symmetry crystal cell, containing 16 symmetry-generated molecules (bottom). Color code: pink: boron; grey: carbon; green: fluorine; light gray: hydrogen; blue: nitrogen; red: oxygen.

ing scheme for the molecule are provided in the ESI.† **2** crystallizes in the orthorhombic crystal system, space group *Fdd*2. The boron atom is coordinated in a tetrahedral geometry by two nitrogen and two fluorine atoms. The BODIPY core is near-planar, and the dihedral angle between the two pyrrole rings is 9.58°. The planarity of the indacene core, which forms an extended conjugated system, is an essential requirement for the optical properties of this class of compounds. The *meso*-phenyl group is nearly orthogonal to the indacene 12-member cycle, with the two moieties forming an angle of 79.9(6)°. This conformation limits the possible resonance between the indacene core and the phenyl ring, as also demonstrated by the rather long [1.505(7) Å] chemical bond between them, a distance consistent with a single bond character. The orientation of the phenyl group allows the formation of a stabilizing CH-π hydrogen bond [2.91 Å] between one of the methyl groups on the indacene core and the centroid of the aromatic ring. The benzoic group orients at an angle of 38.82° relative to the BODIPY core plane and at an angle of 58.96° with respect to the plane of the phenyl group. This last value shows a lack of extensive π-coupling between the two phenyl rings, although partial delocalization involving the carboxylate group is still possible. Indeed, the rather short carboxylic C–O distance [1.406(6) Å] indicates a partial double bond character. The crystal packing of **2** appears to be mainly stabilized by a number of hydrogen bonds between aromatic hydrogen atoms and the fluorine and oxygen atoms in the molecule. Neither the indacene core nor the phenyl rings show any evidence of stabilizing π–π stacking interactions.

The spectroscopic data for compound **2** in various solvents are summarized in Table 1. Briefly, the absorption spectra of **2**

Table 1 Photophysical data of **2** in toluene, dichloromethane (DCM), DMSO and acetonitrile

Solvent	λ_{Abs} [nm]	ε [$\times 10^3$ M^{-1} cm^{-1}]	λ_{Em} [nm]	Stokes shift [nm]	Φ_F
Toluene	504	91.8	517	13	0.60
DCM	502	103.6	516	14	0.57
DMSO	502	86.4	516	14	0.67
Acetonitrile	498	87.5	511	13	0.51

in toluene show an absorption maximum at 504 nm with a molar extinction coefficient of 91.8 × 10^3 M^{-1} cm^{-1}. A minor solvent dependency is observed. In acetonitrile the absorption maximum undergoes a hypsochromic shift of 6 nm to 498 nm. The emission maximum of **2** in toluene is located at 517 nm with a fluorescence quantum yield of 0.60, while the emission maximum in acetonitrile is at 511 nm with a fluorescence quantum yield of 0.51. In comparison, **1** in toluene has an absorption maximum at 503 nm, an emission maximum at 515 nm, and a slightly higher fluorescence quantum yield (0.64).[49] When comparing the absorption spectra of **1** and **2** in acetonitrile, an increased absorption is observed for the latter in the UV-region, with a maximum at 231 nm (Fig. 2). This can be attributed to the absorption of the phenyl group of the benzoic ester moiety. ATR FTIR spectroscopy reveals the presence of a carbonyl stretching band at 1738 cm^{-1} and no –OH functionality (Fig. S2†), corroborating the successful esterification of **1** with benzoic acid, leading to **2**.

Characterization of the CNOs

BODIPY-CNOs were characterized by a wide variety of analytical, spectroscopic and microscopic techniques. Full characterization of the efficiency of nanodiamond conversion and the purity of the **p-CNO**s was obtained using a combination of TGA, LR and HRTEM (with EELS), Raman and FTIR spectroscopy. Similar techniques were used for the characterization of **benz-CNO**s, verifying a successful covalent CNO functionalization with benzoic acid by the *Tour* reaction.

Raman spectroscopy indicated a successful covalent functionalization of the **p-CNO** starting material, reflected as an increase of the D-band at 1320 cm^{-1}, compared to the

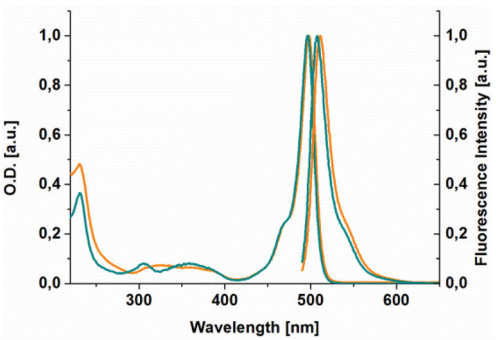

Fig. 2 Normalized absorption (left axis) and fluorescence (right axis) spectra of **1** (green) and **2** (orange) in acetonitrile. Excitation at 485 nm.

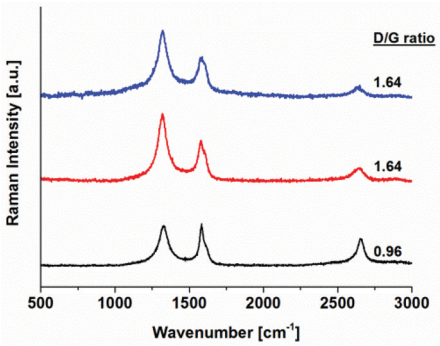

Fig. 3 Raman spectra of **p-CNO**s (black), **benz-CNO**s (red) and **BODIPY-CNO**s (blue). Raman spectra normalized for the G-band at 1580 cm^{-1}, the ratios of the D-band to the G-band intensities are indicated.

G-band at 1580 cm^{-1} (Fig. 3). The D/G ratio increases from 0.96 for the **p-CNO**s to 1.64 for the **benz-CNO**s and for the **BODIPY-CNO**s. FTIR spectroscopy proved the nature of the functional groups introduced based on their characteristic stretching vibrations. While **p-CNO**s showed no significant IR bands, **benz-CNO**s displayed some distinct IR bands in the region between 620 and 1800 cm^{-1}, which changed significantly upon esterification with **1** (Fig. 4). The most distinctive feature is a carbonyl band at around 1640 cm^{-1} (Fig. 4, inset).

Thermogravimetric analysis confirms the successful functionalization of the CNOs (Fig. S3†). **p-CNO**s decompose at around 570 °C, without any weight loss at lower temperatures. **Benz-CNO**s revealed significant weight loss starting at around 150 °C and decomposed completely at around 570 °C as well. In the low temperature domain, the weight loss of **BODIPY-CNO**s was significantly larger due to an increased organic functionalization with BODIPY fluorophores. The degree of functionalization of the CNO nanomaterial was estimated from the weight losses, as described in the literature,[50] assuming that one CNO consists of 6 carbon shells. The TGA of **benz-CNO**s and **BODIPY-CNO**s performed in air shows a weight loss at 400 °C of about 10% and additional 18%, respectively. We estimated about 55 benzoic acid functionalities per onion for **benz-CNO**s and approx. 37 BODIPY molecules per CNO for **BODIPY-CNO**s.

UV-vis-NIR absorption spectroscopy of **BODIPY-CNO**s revealed the typical absorption features of CNOs as a broad plasmonic absorption over the whole spectral range (Fig. 5) and a distinct absorption band, with a maximum at 502 nm in dimethyl sulfoxide (DMSO), which can be attributed to BODIPY. Upon photoexcitation, fluorescence emission with a maximum at 512 nm was observed. Comparison of the maximum fluorescence intensities of a **BODIPY-CNO** dispersion with that of a solution of **2** in DMSO allowed for an estimation of the **BODIPY-CNO**'s fluorescence quantum yield with a value of about 0.17 (*i.e.* 25% of the fluorescence quantum yield of **2**). The BODIPY centered absorption at the excitation wavelength of 490 nm was similar for both samples. All spectroscopic results support the successful covalent functionalization of CNOs with the bright fluorescent BODIPY dye. Notably, while many other dye molecules covalently linked to different carbon nanostructures exhibit a strong fluorescence quenching, which limits their use in imaging applications,[51–53] **BODIPY-CNO**s largely overcome this problem. The attachment of BODIPY to the CNOs leads in fact merely to a small reduction of the fluorescence emission. This fluorescence quenching observed for **BODIPY-CNO**s can be ascribed to the high absorption of the bulk CNO material and not to electron/energy transfer events, which usually result in

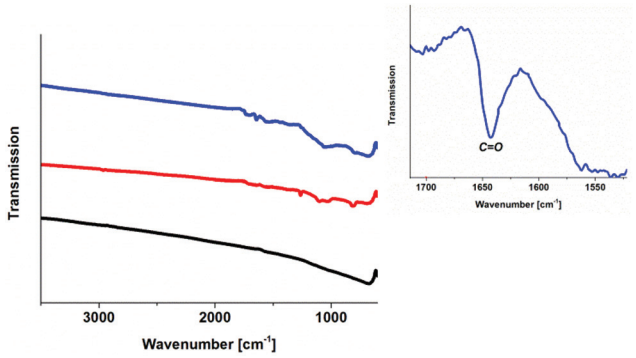

Fig. 4 ATR FTIR spectra of **p-CNO**s (black), **benz-CNO**s (red) and **BODIPY-CNO**s (blue). Inset: magnification of the carbonyl region in the IR-spectrum of **BODIPY-CNO**s.

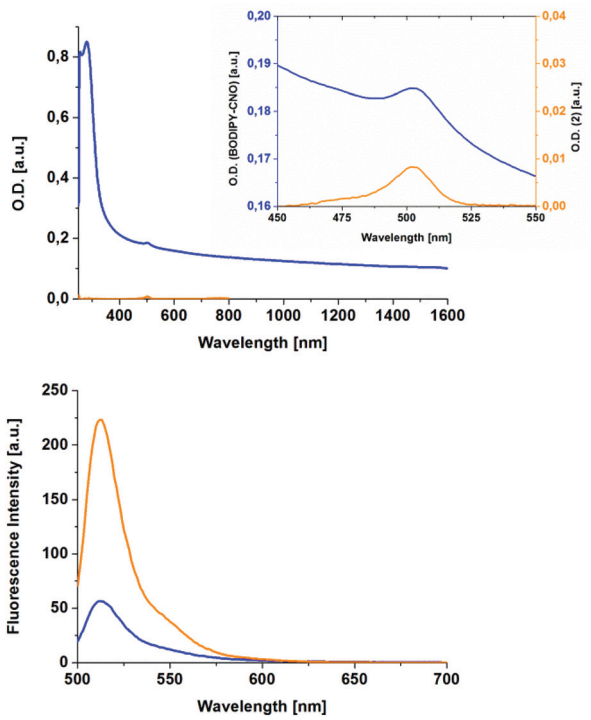

Fig. 5 Absorption spectra (top) and corresponding fluorescence spectra (bottom) of **BODIPY-CNO**s (blue) and **2** (orange) in DMSO. Inset: magnification of the BODIPY centered absorption features in **BODIPY-CNO**s and **2** with comparable BODIPY absorption intensity at the excitation wavelength of 490 nm.

very pronounced fluorescence quenching. These conclusions are consistent with our recent report using NIR fluorescent BF_2-chelates of azadipyrromethene dyes in combination with CNOs,[54] and very promising for the design and application of fluorescent labels based on CNOs for biological imaging.

DLS and Z-potential measurements were performed in order to characterize the nanoparticles' behavior under physiological conditions (Table S2†). DLS measurements were performed in phosphate buffered saline (PBS) at pH 7.4 to mimic the conditions used in biological experiments. Initially, **benz-CNO**s and **BODIPY-CNO**s were dissolved in DMSO at a concentration of 1.0 mg mL^{-1} and then diluted with PBS to a final concentration of 10 μg mL^{-1}. Z-potential measurements were conducted instead in a low ionic strength medium (phosphate buffer 0.01 M, pH 7.4), at a 20 μg mL^{-1} CNO concentration and without prior dispersion in DMSO, in order not to alter the characteristics of their surface. Under these conditions, **BODIPY-CNO** agglomerates show a bimodal dimensional distribution, featuring averages of 110 ± 16 nm (43%) and 426 ± 93 nm (57%), which display a Z-potential of −23 mV. As expected, this value is less negative than the one found for **benz-CNO**s, −39.7 mV.

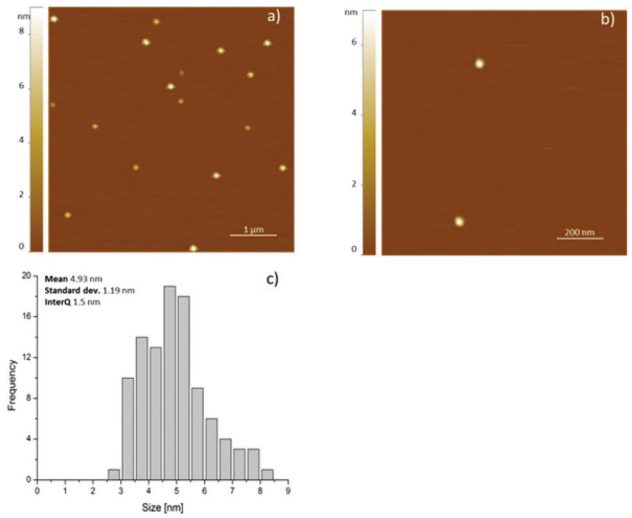

Fig. 6 AFM of **BODIPY-CNO**s. (a) and (b) topographs of CNOs at different magnifications; (c) size distribution analysis.

AFM analyses were performed to estimate the size of the nano-onions. Fig. 6 illustrates two typical topographic images of individual **BODIPY-CNO**s, deposited on mica. The height distribution analysis of about 100 individual CNOs is plotted in Fig. 6c and clearly reveals the predominance of CNOs with an average diameter of 5 nm and a few larger CNOs.

TEM was used to characterize the carbon nanomaterials and confirmed the initial conversion of nanodiamonds to CNOs. The presence of agglomerates of **BODIPY-CNO**s with a size of few hundred nm was confirmed by bright field (BF) TEM investigations (Fig. 7a). HR-TEM analysis shows that individual CNOs have an average diameter of 5–7 nm, with 6–8 concentric graphitic shells, 3.4 Å apart (Fig. 7b and S4†). A few larger particles were found, up to 13 nm and 14 concentric graphitic shells. For all the samples EEL spectra at the carbon K-edge region (270–360 eV energy loss) show the typical near-edge fine structure for CNOs (Fig. 7c and S4†), with a narrow peak corresponding to the 1s→π* transition (285 eV), indicating predominantly sp^2-bonded carbons and a weaker peak at about 292 eV, corresponding to a 1s→σ* transition.[55]

In vitro toxicity investigation and cellular biodistribution of CNOs in MCF-7 cells

In order to investigate the *in vitro* toxicity of different preparations of CNOs, the metabolic activity of MCF-7 cells was determined upon exposure to increasing concentrations of **benz-CNO**s and **BODIPY-CNO**s (from 0.5 to 10 μg mL^{-1}). Cell viability was measured after 24, 48, and 72 hours of incubation using the WST-8 test (Water-Soluble Tetrazolium salt) (Fig. 8). The administration of functionalized CNOs did not affect the

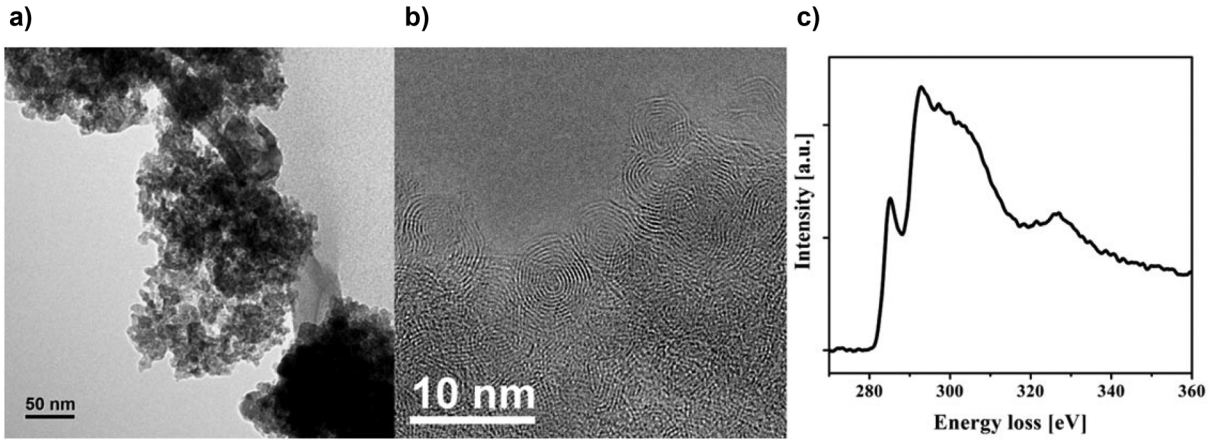

Fig. 7 (a) Overview BF-TEM image of a **BODIPY-CNO** aggregate. (b) HR-TEM image of peripheral **BODIPY-CNO**s in an aggregate partly suspended on a hole. The measured intershell spacing is 3.4 Å. (c) Single-scattering EEL spectrum at the carbon K-edge collected from a **BODIPY-CNO** aggregate suspended under vacuum, showing the typical near-edge fine structure reported for CNOs.[55]

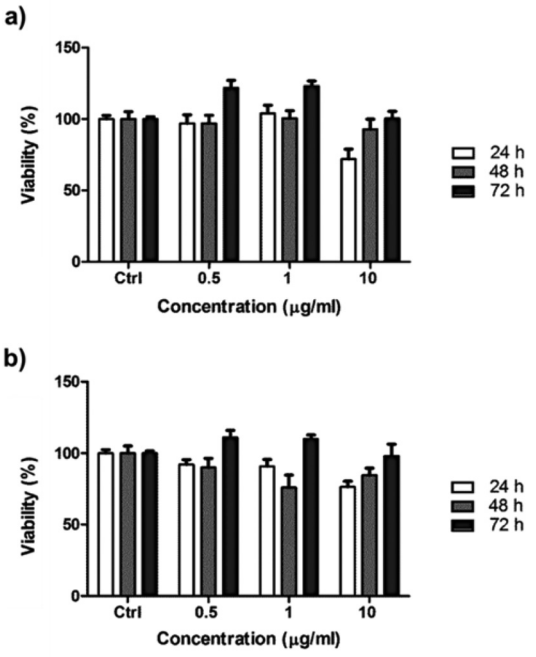

Fig. 8 Cellular viability of MCF-7 cells after exposure to different CNOs. Viability of MCF-7 cells exposed to CNOs was evaluated by the WST-8 assay. Viability of CNO treated cells was expressed relative to non-treated control cells (Ctrl). Viability of cells treated for 24, 48, and 72 hours (a) with 0.5, 1, and 10 μg mL^{-1} **benz-CNOs** and (b) with 0.5, 1, and 10 μg mL^{-1} **BODIPY-CNOs**.

cellular viability as compared with the cell control (Fig. 8a), even after prolonged exposure (72 h) (Fig. 8a and b).

To visualize the intracellular distribution of CNOs, confocal live cell imaging was performed using fluorescent **BODIPY-CNOs**. Representative images of the subcellular localization of **BODIPY-CNOs** (10 μg mL^{-1}) in living MCF-7 cells treated for 48 hours with the nanoparticles are shown in Fig. 9. The CNOs were efficiently taken up by the cells and were found to localize predominantly in the cytoplasm and in the perinuclear region (Fig. 9a and d). To probe the intracellular fate of CNOs in greater detail, the distribution of **BODIPY-CNOs** into vesicular compartments was analyzed in living cells in combination with the Lysotracker probe, a specific marker of lysosomes (Fig. 9b and e). As highlighted by the yellow colocalization signals in Fig. 9c and f, **BODIPY-CNOs** localize in lysosomal vesicles, in line with previous reports on nanoparticles.[56,57] Conversely, unconjugated BODIPY **2** showed only weak staining of cellular membranes (data not shown), as BODIPY is an intrinsically lipophilic fluorescent dye.[58]

The internalization of CNOs in the lysosomes was further studied by colocalization analysis. Fig. S5B† shows the white colocalization mask applied to the image of **BODIPY-CNOs** and lysosomes in Fig. S5A.† The white signal (Fig. S5Ba and b†) represents the overlapping regions of green CNOs and red lysosomal signals that are also represented in the middle area of the scatter plot (Fig. S5Bc†). Pearson's correlation coefficient

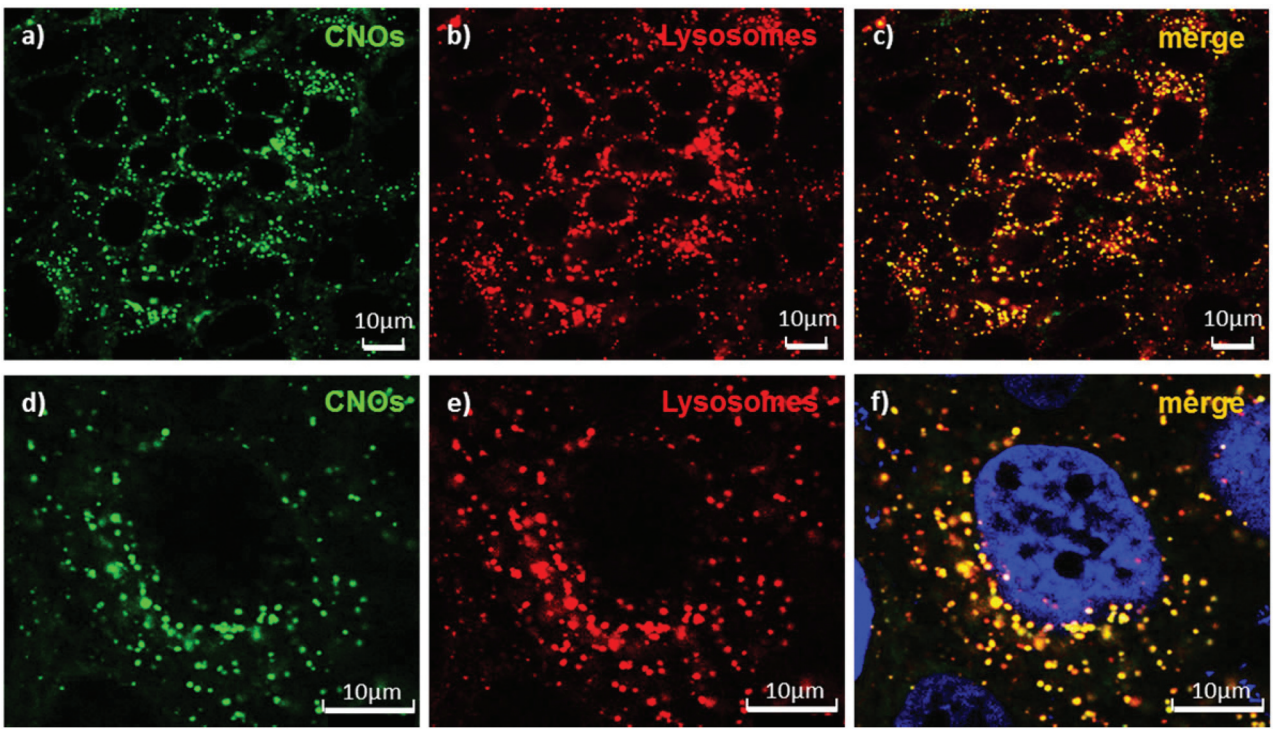

Fig. 9 Cellular uptake of **BODIPY-CNO** nanoparticles visualized by confocal microscopy imaging in living cells. Representative confocal images of MCF-7 cells incubated for 48 hours with 10 μg mL^{-1} **BODIPY-CNOs**. (a–c) Large field of view with several cells, and (d–f) imaging at single cell resolution. (a, d) Green fluorescent **BODIPY-CNOs**, (b, e) lysosomes stained with Lysotracker Red probe, (c) merged images. Hoechst 33342 was used for vital staining of the nucleus (f). Note the high level of **BODIPY-CNO** uptake, and the colocalization (yellow) of the **BODIPY-CNO** within the lysosomes.

(PCC) was used to quantify the degree of colocalization. The PCC measured was 0.7892.

In Fig. S6† some representative stacks of the optical sectioning of a cell incubated with **BODIPY-CNO**s (10 μg mL^{-1}) and Lysotracker are shown. The signal of the internalized CNOs matches with the signal of the lysosomes throughout the volume of the cell. The movie of the complete *z*-stack acquired is shown in the ESI Movie M1.†

In summary, the presented data verify that CNOs can abundantly enter cells without exerting toxic effects on the investigated MCF-7 cells (although further studies are needed to completely elucidate this point). The CNO nanomaterials are internalized by endocytosis and do not enter the nucleus of the cells.

Conclusions

Boron dipyrromethene (BODIPY) functionalized CNO conjugates have been synthesized and characterized. The high fluorescence of the nanoparticles allowed high-resolution imaging in MCF-7 human breast cancer cells. The CNOs were efficiently taken up by the cells and localized in lysosomes. Cell viability measured up to 72 hours following incubation did not show significant cytotoxicity. BODIPY-CNO conjugates have the necessary characteristics for further development of theranostic nano-platforms which combine targeting, imaging and therapeutic capabilities, due to their low cytotoxicity and the low fluorescence quenching of the attached fluorescence probes. In combination with the synthetic versatility of BODIPY dyes, CNOs are very promising for the future preparation of nanomaterials with tailor-made photophysical properties for various biological and theranostic applications.

Experimental

Materials and methods

All starting materials, reagents and solvents were purchased from Sigma-Aldrich in high-purity grade and used without further purification. Spectrophotometric or HPLC grade solvents were used for UV-vis and fluorescence studies. All measurements were performed at room temperature and under ambient conditions, unless otherwise noted. All instrumental details and additional procedures are summarized in the ESI.†

Synthetic procedures

1: BODIPY fluorophore **1** was synthesized following a previously published procedure.[43]

2: Benzoic acid (122.1 mg/1.00 mmol), NHS (115.1 mg/1.00 mmol), DCC (206.3 mg/1.00 mmol) and DMAP (122.2 mg/1.00 mmol) were dissolved in 40 mL of dry THF at 0 °C under a N_2 atmosphere. The solution was allowed to warm up to room temperature and stirred for another 5 h. Then, **1** (67 mg/0.20 mmol) dissolved in 10 mL of dry, deoxygenated THF was added and the reaction mixture was stirred at room temperature for 5 days. The solution was filtered and after evaporation of the THF, the crude product was purified by column chromatography (SiO_2, hexane–dichloromethane (DCM) 3 : 1 (v/v) with rising amounts of DCM). **2** was obtained as a bright orange solid in 33% yield (29 mg/0.065 mmol). X-ray quality crystals were obtained as orange rhombic plates by re-crystallizing from dichloromethane–methanol 1 : 3 (v/v) in the freezer (−20 °C). ^{1}H NMR (400 MHz, $CDCl_3$) δ 8.23 (d, 2H, J = 8.3 Hz), 7.67 (t, 1H, J = 7.5 Hz), 7.54 (t, 2H, J = 7.8 Hz), 7.37 (m, 4H), 6.01 (s, 2H), 2.57 (s, 6H), 1.48 (s, 6H). ^{13}C NMR (100 MHz, $CDCl_3$) (14.6, 121.4, 122.7, 126.6, 128.6, 128.7, 129.3, 130.2, 131.5, 132.6, 133.9, 140.1, 143.2, 151.6, 155.8). HRMS-ESI: m/z: calcd for $C_{26}H_{24}BF_2N_2O_2^+$: 445.1899 $[M + H]^+$, found: 445.1911.

Benz-CNO: $NaNO_2$ (1.47 g/21.3 mmol) was dissolved in 20 mL deionized (DI) water and cooled to 0 °C. This solution was added at once to a solution of 4-aminobenzoic acid (2.88 g/21.0 mmol) in 30 mL DMF at 0 °C. Conc. HCl (200 μL) was added and the mixture was stirred for 30 min at 0 °C. **p-CNOs**[44–46] (31 mg) were dispersed in 20 mL DMF by ultrasonication for 20 min and the dispersion was added to the reaction mixture, which was stirred at 0 °C for 4 h and at RT for additional 3 days. Following this, the CNOs were separated from the reaction mixture by centrifugation (30 min, 2100*g*) and purified by subsequent re-dispersion – centrifugation steps in DI water, DMF, and methanol. After drying at 60 °C overnight, 25 mg of **benz-CNO**s were recovered.

BODIPY-CNO: **Benz-CNO**s (10 mg) were dispersed in 20 mL dry THF and the dispersion was deoxygenated with N_2. Then NHS (9.2 mg/0.08 mmol), DMAP (12.0 mg/0.08 mmol) and EDC (12.4 mg/14 μL/0.08 mmol) were added and the mixture was heated under reflux for 1 h. Following this, **1** (13.6 mg/0.04 mmol) was added and the reaction mixture was heated for another 44 h under reflux. After cooling to room temperature, the CNOs were precipitated by centrifugation (30 min/2100*g*) and separated from the supernatant. Subsequently, the solid was re-dispersed by brief ultrasonication in THF and again centrifuged. This process was repeated four more times. The obtained solid was dried at 60 °C overnight. Approx. 12 mg of **BODIPY-CNO**s were recovered.

CNO preparation for cellular studies. **Benz-** and **BODIPY-CNOs** were dispersed in DMSO (1 mg mL^{-1}) and intensively sonicated as previously described.[23] For cellular *in vitro* experiments, all CNOs preparations were sonicated for 15 min at 50 kHz (100% intensity), diluted to the desired concentrations in a cell culture medium (DMEM), and sonicated for 15 min at 50 kHz before adding to the cells.

Cell cultures. MCF-7 cells (human mammary gland adenocarcinoma cell line ATCC HTB-22) were cultivated in DMEM with 50 μM glutamine, supplemented with 10% FBS, 100 U mL^{-1} penicillin and 100 mg mL^{-1} streptomycin. Cells were incubated in a humidified and controlled atmosphere with a 95% to 5% ratio of air/CO_2, at 37 °C.

WST-8 assay. MCF-7 cells were seeded in 96 well microplates at a density of 5000 cells per well at a final volume of 100 μl and incubated for 24 h in a humidified atmosphere at 37 °C

and 5% CO_2 to obtain a subconfluent monolayer (60–70% of confluence). The culture medium was removed and replaced with 100 μl of medium containing CNOs at the final concentrations of 0.5, 1, and 10 μg mL^{-1}. The metabolic activity of all cultures was determined after 24, 48 and 72 h of exposure to CNOs, using a standard WST-8 assay (Sigma). Assays were performed following the procedure previously described.[59] Data were expressed as mean ± SD. Differences in cell proliferation between cells treated with CNOs and the control were considered statistically significant with a p-value <0.05.

Confocal microscopy. Fluorescence imaging was performed with a SP8-STED microscope (Leica Microsystems, GmbH, Germany) using a 63× oil immersion objective (HC PL APO CS2 63×/1.40 OIL). **BODIPY-CNOs** were excited at 488 nm and the emission was acquired in the spectral window at 500–560 nm. Lysosomes were imaged by exciting the LysoTracker Red DND-99 with the 577 nm line of the white light laser (WLL, Leica), and acquired in the emission range of 600–680 nm. The nucleus stained with Hoechst 33342 (Sigma) was excited with the 405 nm wavelength and acquired at 415–480 nm.

CNOs incubation for cellular imaging. MCF-7 cells were seeded in 3.5 cm glass bottom dishes (World Precision Instruments, FD35-100) and incubated for 24 h in a humidified atmosphere at 37 °C and 5% CO_2 to obtain a subconfluent monolayer (60–70% of confluence). After 24 h the medium was removed, and the cells were incubated with a suspension of **BODIPY-CNOs** (10 μg mL^{-1}). As a control, cells were left untreated (not shown). After 48 h of incubation at 37 °C with CNOs, the cells were washed three times with PBS (pH 7.4) and incubated for 30 minutes with 75 nM LysoTracker Red DND-99 (L7528, Life Technologies). The medium was then replaced with a fresh medium and the cells were transferred to the microscope incubator (Life Imaging Services, Switzerland). The temperature was maintained at 37 °C using the Cube and Box temperature control system, and the humidified 5% CO_2 atmosphere was maintained using an automated gas mixer system (The Brick; Life Imaging Services).

Acknowledgements

We are grateful to the Istituto Italiano di Tecnologia (IIT) for funding. The authors wish to thank Dr Agustin Molina-Ontario (UTEP) for the preparation of the pristine CNOs; Dr Marco Frasconi, Dr Marco Salerno, Dr Farouk Ayadi, Sine Mandrup Bertozzi, Giammarino Pugliese (IIT Genova) for instrumental support and helpful discussions. LE wishes to thank the NSF, PREM Program (DMR-1205302) and the Robert A. Welch Foundation (Grant AH-0033) for generous support.

Notes and references

1 C. Fabbro, H. Ali-Boucetta, T. Da Ros, K. Kostarelos, A. Bianco and M. Prato, *Chem. Commun.*, 2012, **48**, 3911.
2 B. S. Wong, S. L. Yoong, A. Jagusiak, T. Panczyk, H. K. Ho, W. H. Ang and G. Pastorin, *Adv. Drug Delivery Rev.*, 2013, **65**, 1964.
3 N. Saito, H. Haniu, Y. Usui, K. Aoki, K. Hara, S. Takanashi, M. Shimizu, N. Narita, M. Okamoto, S. Kobayashi, H. Nomura, H. Kato, N. Nishimura, S. Taruta and M. Endo, *Chem. Rev.*, 2014, **114**, 6040.
4 A. Montellano, T. Da Ros, A. Bianco and M. Prato, *Nanoscale*, 2011, **3**, 4035.
5 J. Luczkowiak, A. Munoz, M. Sanchez-Navarro, R. Ribeiro-Viana, A. Ginieis, B. M. Illescas, N. Martin, R. Delgado and J. Rojo, *Biomacromolecules*, 2013, **14**, 431.
6 J. Shi, X. Yu, L. Wang, Y. Liu, J. Gao, J. Zhang, R. Ma, R. Liu and Z. Zhang, *Biomaterials*, 2013, **34**, 9666.
7 Z. Liu, S. Tabakman, K. Welcher and H. Dai, *Nano Res.*, 2009, **2**, 85.
8 K. Kostarelos, A. Bianco and M. Prato, *Nat. Nanotechnol.*, 2009, **4**, 627.
9 V. N. Mochalin, O. Shenderova, D. Ho and Y. Gogotsi, *Nat. Nanotechnol.*, 2012, **7**, 11.
10 Y. Zhu, J. Li, W. Li, Y. Zhang, X. Yang, N. Chen, Y. Sun, Y. Zhao, C. Fan and Q. Huang, *Theranostics*, 2012, **2**, 203.
11 H. Zhang, G. Grüner and Y. Zhao, *J. Mater. Chem. B*, 2013, **1**, 2542.
12 L. Feng, L. Wu and X. Qu, *Adv. Mater.*, 2013, **25**, 168.
13 D. Ugarte, *Nature*, 1992, **359**, 707.
14 L. Echegoyen, A. Ortiz, M. N. Chaur and A. J. Palkar, in *Chemistry of Nanocarbons*, ed. T. Akasaka, F. Wudl and S. Nagase, John Wiley & Sons, Chichester, UK, 2010, pp. 463–483.
15 A. Hirata, M. Igarashi and T. Kaito, *Tribol. Int.*, 2004, **37**, 899.
16 L. Joly-Pottuz, N. Matsumoto, H. Kinoshita, B. Vacher, M. Belin, G. Montagnac, J. M. Martin and N. Ohmae, *Tribol. Int.*, 2008, **41**, 69.
17 J. Luszczyn, M. E. Plonska-Brzezinska, A. Palkar, A. T. Dubis, A. Simionescu, D. T. Simionescu, B. Kalska-Szostko, K. Winkler and L. Echegoyen, *Chem. – Eur. J.*, 2010, **16**, 4870.
18 J. Breczko, M. E. Plonska-Brzezinska and L. Echegoyen, *Electrochim. Acta*, 2012, **72**, 61.
19 N. Keller, N. I. Maksimova, V. V. Roddatis, M. Schur, G. Mestl, Y. V. Butenko, V. L. Kuznetsov and R. Schlögl, *Angew. Chem., Int. Ed.*, 2002, **41**, 1885.
20 D. Pech, M. Brunet, H. Durou, P. Huang, V. Mochalin, Y. Gogotsi, P.-L. Taberna and P. Simon, *Nat. Nanotechnol.*, 2010, **5**, 651.
21 Y. Gao, Y. S. Zhou, M. Qian, X. N. He, J. Redepenning, P. Goodman, H. M. Li, L. Jiang and Y. F. Lu, *Carbon*, 2013, **51**, 52.
22 M. E. Plonska-Brzezinska, D. M. Brus, A. Molina-Ontaria and L. Echegoyen, *RSC Adv.*, 2013, **3**, 25891.
23 M. Yang, K. Flavin, I. Kopf, G. Radics, C. H. A. Hearnden, G. J. McManus, B. Moran, A. Villalta-Cerdas, L. A. Echegoyen, S. Giordani and E. C. Lavelle, *Small*, 2013, **9**, 4194.
24 P. Singh, S. Campidelli, S. Giordani, D. Bonifazi, A. Bianco and M. Prato, *Chem. Soc. Rev.*, 2009, **38**, 2214.

25 K. Flavin, M. N. Chaur, L. Echegoyen and S. Giordani, *Org. Lett.*, 2010, **12**, 840.
26 J. L. Bahr, J. Yang, D. V. Kosynkin, M. J. Bronikowski, R. E. Smalley and J. M. Tour, *J. Am. Chem. Soc.*, 2001, **123**, 6536.
27 A. Loudet and K. Burgess, *Chem. Rev.*, 2007, **107**, 4891.
28 G. Ulrich, R. Ziessel and A. Harriman, *Angew. Chem., Int. Ed.*, 2008, **47**, 1184.
29 Q. Zheng, G. Xu and P. N. Prasad, *Chem. – Eur. J.*, 2008, **14**, 5812.
30 K. E. Beatty, J. Szychowski, J. D. Fisk and D. A. Tirell, *ChemBioChem*, 2011, **12**, 2137.
31 A. Romieu, C. Massif, S. Rihn, G. Ulrich, R. Ziessel and P.-Y. Renard, *New J. Chem.*, 2013, **37**, 1016.
32 C. Y. Lee and J. T. Hupp, *Langmuir*, 2010, **26**, 3760.
33 O. A. Bozdemir, S. Erbas-Cakmak, O. O. Ekiz, A. Dana and E. U. Akkaya, *Angew. Chem., Int. Ed.*, 2011, **50**, 10907.
34 J. Iehl, J.-F. Nierengarten, A. Harriman, T. Bura and R. Ziessel, *J. Am. Chem. Soc.*, 2012, **134**, 988.
35 M. E. El-Khouly, S. Fukuzumi and F. D'Souza, *ChemPhysChem*, 2014, **15**, 30.
36 J. Bartelmess, A. J. Francis, K. A. El Roz, F. N. Castellano, W. W. Weare and R. D. Sommer, *Inorg. Chem.*, 2014, **53**, 4527.
37 S. G. Awuah and Y. You, *RSC Adv.*, 2012, **2**, 11169.
38 A. Kamkaev, S. H. Lim, H. B. Lee, L. V. Kiew, L. Y. Chung and K. Burgess, *Chem. Soc. Rev.*, 2013, **42**, 77.
39 A. B. Nepomnyashchii and A. J. Bard, *Acc. Chem. Res.*, 2012, **45**, 1844.
40 N. Boens, V. Leen and W. Dehaen, *Chem. Soc. Rev.*, 2012, **41**, 1130.
41 K. Krumova and G. Cosa, *J. Am. Chem. Soc.*, 2010, **132**, 17560.
42 J. Bartelmess, W. W. Weare, N. Latortue, C. Duong and D. S. Jones, *New J. Chem.*, 2013, **37**, 2663.
43 J. Bartelmess and W. W. Weare, *Dyes Pigm.*, 2013, **97**, 1–8.
44 V. L. Kuznetsov, M. N. Aleksandrov, I. V. Zagoruiko, A. L. Chuvilin, E. M. Moroz and V. N. Kolomiichuk, *Carbon*, 1991, **29**, 665.
45 V. L. Kuznetsov, A. L. Chuvilin, Y. V. Butenko, I. Y. Mal'kov and V. M. Titov, *Chem. Phys. Lett.*, 1994, **222**, 343.
46 A. Palkar, F. Melin, C. M. Cardona, B. Elliott, A. K. Naskar, D. D. Edie, A. Kumbhar and L. Echegoyen, *Chem. – Asian J.*, 2007, **2**, 625.
47 J. Bartelmess, B. Ballesteros, G. de la Torre, D. Kiessling, S. Campidelli, M. Prato, T. Torres and D. M. Guldi, *J. Am. Chem. Soc.*, 2010, **132**, 16202.
48 K. Flavin, K. Lawrence, J. Bartelmess, M. Tasior, C. Navio, C. Bittencourt, D. F. O'Shea, D. M. Guldi and S. Giordani, *ACS Nano*, 2011, **2**, 1198.
49 T. Lazarides, S. Kuhri, G. Charalambidis, M. K. Panda, D. M. Guldi and A. G. Coutselos, *Inorg. Chem.*, 2012, **51**, 4193.
50 C. T. Cioffi, A. Palkar, F. Melin, A. Kumbhar, L. Echegoyen, M. Melle-Franco, F. Zerbetto, G. M. A. Rahman, C. Ehli, V. Sgobba, D. M. Guldi and M. Prato, *Chem. – Eur. J.*, 2009, **15**, 4419.
51 V. V. Didenko, V. C. Moore, D. S. Baskin and R. E. Smalley, *Nano Lett.*, 2005, **5**, 1563.
52 B. Tian, C. Wang, S. Zhang, L. Feng and Z. Liu, *ACS Nano*, 2011, **5**, 7000.
53 Y. Liu, C.-y. Liu and Y. Liu, *Appl. Surf. Sci.*, 2011, **257**, 5513.
54 S. Giordani, J. Bartelmess, M. Frasconi, I. Biondi, S. Cheung, M. Grossi, D. Wu, L. Echegoyen and D. F. O'Shea, *J. Mater. Chem. B*, 2014, DOI: 10.1039/C4TB01087F.
55 P. Redlich, F. Banhart, Y. Lyutovich and P. M. Ajayan, *Carbon*, 1998, **36**, 561.
56 S. Sabella, R. P. Carney, V. Brunetti, M. A. Malvindi, N. Al-Juffali, G. Veccio, S. M. Janes, O. M. Bakr, R. Cingolani, F. Stellacci and P. P. Pompa, *Nanoscale*, 2014, **6**, 7052.
57 G. Leménager, E. De Luca, Y.-P. Sun and P. P. Pompa, *Nanoscale*, 2014, **6**, 8617.
58 *The Molecular Probes® Handbook—A Guide to Fluorescent Probes and Labeling Technologies*, ed. I. Johnson and M. T. Z. Spence, Life Technologies Corporation, Carlsbad (CA), 10th edn, 2010.
59 M. A. Malvindi, V. Brunetti, G. Vecchio, A. Galeone, R. Cingolani and P. P. Pompa, *Nanoscale*, 2012, **4**, 486.